# Hierarchical Optimal Control of the Resilient Community Microgrid in Islanded Mode

Jimiao zhang<sup>1</sup>, Jie Li<sup>1</sup>, Lei Wu<sup>2</sup>, Melike Erol-Kantarci <sup>3</sup>, Burak Kantarci <sup>3</sup>

Electrical and Computer Engineering, Clarkson University, Potsdam, NY, USA (jimzhan, jieli@clarkson.edu)
Electrical and Computer Engineering, Stevens Institute of Technology, Hoboken, NJ, USA (lei.wu@stevens.edu)

Abstract—This paper studies a three-level hierarchical control strategy for the resilient community underground microgrid in Potsdam, NY, operated in the islanded mode. Specifically, an AC Optimal Power Flow (ACOPF) problem is solved via rank-relaxed semidefinite programming (SDP) method on the tertiary level to derive an optimal operating point of the microgrid. Two decentralized secondary control methods based on proportional-integral (PI) control are proposed, one is to make PI controllers continually act and the other is to periodically reset the PI outputs to zero. Both methods allow distributed generation (DG) units to closely track the optimal economic dispatch commands by generating frequency correction terms to the primary P-f droop controllers. Simulation studies are carried out with PSCAD/EMTDC, where the proposed methods are compared.

Index Terms—Three-level hierarchical control, AC optimal power flow, optimal operation, droop control.

#### I. INTRODUCTION

Microgrids are localized low or medium voltage distribution networks that consist of an aggregation of distributed energy resources (DER) and energy storage systems, supplying power to a group of local electrical loads. A fully-fledged microgrid has the capability to automatically and smoothly connect to and disconnect from the bulk power grid. With a mix of on-site DERs and energy storage assets, it can be operated as a controllable load in grid-connected mode. In addition, when power failures occur on the main grid, a microgrid could quickly island itself and operate independently. Moreover, operation of microgrids entails a smooth transition between the two modes. With these prominent features, microgrid technologies have emerged as a leading solution that enhances system resiliency, reliability, security, and sustainability for energy producers and consumers alike. Potential benefits of a microgrid also include lower greenhouse gas emissions and reduced stress on electrical transmission and distribution systems.

This paper focuses on the optimal control of the Potsdam resilient underground microgrid operated in the islanded mode. The design of this resilient microgrid intends to provide reliable power for essential services and to allow Potsdam to act as a power hub for emergency operations during North Country disaster conditions [1-2]. Under this

background, electric power would be distributed by underground cables owned by National Grid and supplied only to entities that would provide essential services for disaster response and recovery. It is worth noting that the centralized energy management system (EMS) is particularly suitable for this paradigm due to its system observability and consistent objectives [3]. In islanded mode, distributed generation (DG) units are required to properly share the loads of the microgrid. Furthermore, the system frequency and bus voltages should remain within permissible limits. It is also essential that constraints, such as line flow limits and power balance, will not be violated.

To meet the above control objectives along with the economic targets, the well-known three-level hierarchical scheme [4] is adopted in this paper. The bandwidth of communication channels on the three control levels may vary by at least one order of magnitude, as dynamic response slows down from the primary to the tertiary level. Thus, the three-level scheme would facilitate the decoupling of system dynamics and make the modeling and analysis of a microgrid easier. Specifically, the primary level is mainly concerned with the stability of voltage and frequency. To provide flexible power sharing, the decentralized P - f droop-based control has been extensively implemented. The secondary control level aims to eliminate frequency and voltage deviations caused by the droop-based control, which can also handle voltage unbalance as well as harmonic compensation. It is noteworthy that the above two control levels would be suffice to guarantee secure operation of a microgrid in islanded mode [5], whereas economic dispatch of DERs necessitates the tertiary level. To this end, this study considers the tertiary level and concentrates on AC Optimal Power Flow (ACOPF) problem. ACOPF seeks an optimal operating point to minimize a certain cost function such as total generation cost or line losses, subject to physical constraints on power and voltage variables [6].

Ever since first proposed by Carpentier in 1962, there has been a growing body of research on solving the ACOPF problem. This problem is, by nature, highly non-convex due to the quadratic relationship between voltages and active/ reactive power injections. Early works on ACOPF include

<sup>3.</sup> School of Electrical Engineering and Computer Science, University of Ottawa, Ottawa, Canada (melike.erolkantarci, Burak.Kantarci@uottawa.ca)

Newton-based approaches, linear and quadratic programming, nonlinear programming, alongside other algorithms such as interior point methods and heuristic optimization strategies. However, none of the above solution methods guarantee global optimality. To obtain a global optimum, X. Bai et al. in [7] are the first to propose a semidefinite programming (SDP) relaxation method in power system applications. Later on, a seminal work [8] forms the theoretical basis for applying SDP relaxation to the ACOPF problem. When the only non-convex constraint (i.e. the rank one condition) in the SDP formulation is dropped, convex optimization theory can be applied to the convexified problem to identify global optimal solutions. To date, it has been mathematically proved that this convex relaxation method ensures global optimality for tree networks [9] and also for a group of mesh networks under certain assumptions [8]. In this paper, we leverage the rank relaxation method to solve the ACOPF problem, which determines the optimal operation of DGs with the minimum total operating cost.

The remainder of this paper is organized as follows: Section II presents the hierarchical control mechanism and also discusses coordination among the three layers. Section III briefly introduces the architecture of the resilient underground microgrid in Potsdam, which is later used as the test system. In Section IV the test system is modeled in the PSCAD/EMTDC simulation environment to derive simulation results. Section V concludes the work.

#### II. HIERARCHICAL CONTROL SCHEME

## A. Primary Droop Control Level

To autonomously share power among multiple DGs in islanded mode, the conventional P - f droop curve is introduced to local controllers as in (1). Likewise, reactive power sharing is achieved via Q - V droop control as in (2).

$$\omega_i = \omega_i^* - m_{pi} P_i \tag{1}$$

$$v_{di} = V_i^* - m_{qi}Q_i; \qquad v_{qi} = 0$$
 (2)

Here,  $\omega_i^*$  and  $V_i^*$  respectively denote the nominal angular frequency and voltage amplitude of DG i. The output voltage vector after Park Transformation is controlled to be aligned with the d-axis of the power converter reference frame using a phase-locked loop (PLL) module.  $P_i$  and  $Q_i$  are the filtered active and reactive power injections from DG i. A well-cited pioneering paper [10] has shown that the static droop gains  $m_{pi}$  and  $m_{qi}$  especially  $m_{pi}$ , could significantly impact microgrid stability. For simplicity, this study does not treat droop gains as decision variables on the later tertiary level. Instead, they are set as fixed values as in [10].

# B. Secondary Control Level

While enabling plug-and-play operation and power sharing, the decentralized droop controllers could cause bus voltages and the steady-state network frequency to deviate from their nominal values [11]. Thus, the local secondary

control action is required for each DG to mitigate the aforementioned deviations in both global frequency and local voltage. On the secondary level, it only involves shifting P-fand Q - V curves vertically and thus will not affect the pre-set droop gains. In order to realize decoupling from the primary control level, the secondary control is usually designed with a lower control bandwidth. In this paper frequency restoration is realized by generating a correction term  $\delta \omega$ , to the nominal angular frequency  $\omega_i^*$  using a proportional-integral (PI) controller as in (3).  $K_{c\omega}$  is controller gain,  $\tau_{I\omega}$  is integral time constant, and  $P_i^*$  is active power reference calculated from the tertiary level. The same principle also applies to voltage restoration, as shown in (4). Since frequency is an uncontrollable quantity here, periodical reset action can be enabled in the PI controllers. Alternatively, (3) can be disabled when frequency exceeds its limits.

$$\delta\omega_i = K_{c\omega}(P_i^* - P_i) + \left(K_{c\omega}/\tau_{I\omega}\right) \int (P_i^* - P_i)dt \tag{3}$$

$$\delta v_i = K_{cv} (V_i^* - V_i) + (K_{cv} / \tau_{Iv}) \int (V_i^* - V_i) dt \tag{4}$$

# C. Tertiary Control Level

The EMS can perform the tertiary control by implementing a single-objective or multi-objective optimization [12]. It is industry practice that, at regular intervals of time, optimization is executed. The time span may be one day, one hour, or every 15 minutes. Information pertaining to load and renewable generation forecasts is telemetered to the EMS wherein the economical operation of microgrid is optimized. Control signals, i.e., active and/or reactive power point settings, are then transmitted via the same telemetering channels to dispatchable DGs for implementing the secondary control.

We formulate the ACOPF with voltages in rectangular form. Consider an n-bus distribution network, where  $\mathbf{N} = \{1, 2, ...n\}$  denotes the set of buses,  $\mathbf{G}$ ,  $\mathbf{R}$ ,  $\mathbf{D}$ , and  $\mathbf{L}$  respectively represent sets of conventional DGs, renewable DGs, loads, and lines. Lines are modeled as  $\Pi$ -equivalent circuits, and  $\mathbf{Y} = \mathbf{G} + j\mathbf{B}$  denote the network bus admittance matrix.

Let  $e_k$  in  $\mathbb{R}^n$  represent a standard basis vector with all zeros except the kth element being 1. Define matrices  $Y_k = e_k$ .

$$e_k^T \cdot \mathbf{Y}$$
 and  $Y_{lm} = (y_{lm} + \frac{jb_{lm}}{2})e_l \cdot e_l^T - y_{lm}e_l \cdot e_m^T$ , where  $y_{lm}$  is

series admittance and  $b_{lm}$  is total shunt susceptance of line  $(l, m) \in L$ .  $S_{lm}$  is apparent power flowing along line (l, m). The following matrices are employed in the SDP formulation. Admittance matrices (5)-(6) are defined to calculate power injections, admittance matrices (7)-(8) are used to calculate line flows, and matrix (9) is used to facilitate the calculation of bus voltage magnitudes.

$$\mathbf{Y}_{k} = \frac{1}{2} \begin{bmatrix} \operatorname{Re}(Y_{k} + Y_{k}^{T}) & \operatorname{Im}(Y_{k}^{T} - Y_{k}) \\ \operatorname{Im}(Y_{k} - Y_{k}^{T}) & \operatorname{Re}(Y_{k} + Y_{k}^{T}) \end{bmatrix}$$
 (5)

$$\overline{\mathbf{Y}}_{k} = -\frac{1}{2} \begin{bmatrix} \operatorname{Im}(Y_{k} + Y_{k}^{T}) & \operatorname{Re}(Y_{k} - Y_{k}^{T}) \\ \operatorname{Re}(Y_{k}^{T} - Y_{k}) & \operatorname{Im}(Y_{k} + Y_{k}^{T}) \end{bmatrix}$$
(6)

$$\mathbf{Y}_{lm} = \frac{1}{2} \begin{bmatrix} \text{Re}(Y_{lm} + Y_{lm}^T) & \text{Im}(Y_{lm}^T - Y_{lm}) \\ \text{Im}(Y_{lm} - Y_{lm}^T) & \text{Re}(Y_{lm} + Y_{lm}^T) \end{bmatrix}$$
(7)

$$\overline{\mathbf{Y}}_{lm} = -\frac{1}{2} \begin{bmatrix} \operatorname{Im}(Y_{lm} + Y_{lm}^T) & \operatorname{Re}(Y_{lm} - Y_{lm}^T) \\ \operatorname{Re}(Y_{lm}^T - Y_{lm}) & \operatorname{Im}(Y_{lm} + Y_{lm}^T) \end{bmatrix}$$
(8)

$$\mathbf{M}_{k} = \begin{bmatrix} e_{k}e_{k}^{T} & \mathbf{0} \\ \mathbf{0} & e_{k}e_{k}^{T} \end{bmatrix} \tag{9}$$

The voltage vector is defined as in (10), where  $V_{dk}$  and  $V_{qk}$  are real and imaginary parts of complex voltage at bus k.

$$\mathbf{V} = \begin{bmatrix} V_{d1} & V_{d2} & \cdots & V_{dn} & V_{q1} & V_{q2} & \cdots & V_{qn} \end{bmatrix}^T$$
 (10)

Finally, with the variable substitution defined in (11), the SDP relaxed ACOPF model can be describes as in (12) by neglecting the rank one constraint. If solution to the relaxed model (12) is rank one, it implies solution exactness and the globally optimal voltage profile can be recovered [8].

$$\mathbf{W} = \mathbf{V} \cdot \mathbf{V}^T \tag{11}$$

$$\min_{\mathbf{W}} \sum_{g \in \mathbf{G} \cup \mathbf{R}} \beta_g \tag{12.1}$$

$$\begin{bmatrix} \beta_g - c_{gl} \cdot P_g - c_{g0} & -\sqrt{c_{g2}} \cdot P_g \\ -\sqrt{c_{g2}} \cdot P_g & 1 \end{bmatrix} \succeq 0, \quad g \in G \quad (12.2)$$

$$\beta_{\sigma} = C_{\sigma 1} \cdot [(1 + \eta_{\sigma}) \cdot P_{\sigma}], \quad g \in G$$
 (12.3)

$$P_g^{\min} \le P_g \le P_g^{\max}, \quad g \in \mathbf{G} \cup \mathbf{R}$$
 (12.4)

$$\operatorname{trace}(\mathbf{Y}_k \cdot \mathbf{W}) = \sum_{g \in G_k \cup R_k} P_g - \sum_{d \in D_k} P_d, \quad k \in \mathbb{N}$$
 (12.5)

$$\sum_{g \in G_k \cup R_k} Q_g^{min} \le \operatorname{trace}(\overline{\mathbf{Y}}_k \cdot \mathbf{W}) + \sum_{d \in D_k} Q_d \le \sum_{g \in G_k \cup R_k} Q_g^{max} \quad (12.6)$$

$$(V_k^{\min})^2 \le \operatorname{trace}(\mathbf{M}_k \cdot \mathbf{W}) \le (V_k^{\max})^2, \quad k \in \mathbf{N}$$
 (12.7)

$$\begin{bmatrix} (S_{lm}^{\text{mex}})^2 & -\text{trace}(\mathbf{Y}_{lm} \cdot \mathbf{W}) & -\text{trace}(\mathbf{\overline{Y}}_{lm} \cdot \mathbf{W}) \\ -\text{trace}(\mathbf{Y}_{lm} \cdot \mathbf{W}) & 1 & 0 \\ -\text{trace}(\mathbf{\overline{Y}}_{lm} \cdot \mathbf{W}) & 0 & 1 \end{bmatrix} \succeq 0, \quad (l, m) \in \mathbf{L} \quad (12.8)$$

The objective function (12.1) is to minimize the total operation cost of the microgrid in islanded mode. The quadratic generator cost is considered for a conventional DG  $g \in G$ , where  $C_{g2}$ ,  $C_{g1}$ , and  $C_{g0}$  are respectively the quadratic, linear, and constant coefficients. The scalar  $\beta_g$  is introduced as an auxiliary variable such that the cost functions can be converted to (12.2) via the Schur complement technique. A linear cost function (12.3) is used for a renewable DG  $g \in \mathbb{R}$ , and  $\eta_g$  represents power converter loss factor. Inequality (12.4) represents real power generation capacity limits of individual DGs. Constraints (12.5) and (12.6) enforce real and reactive power

requirements at each bus, whereas constraint (12.7) imposes bus voltage magnitude limits. The apparent power line flow limits are expressed as in constraint (12.8) via the Schur complement formula. Constraint (12.9) requires the square variable matrix **W** to be positive semidefinite.

# D. Coordination among The Three Levels

Practical microgrids adopt hierarchical control schemes so as to meet the desired operational requirements. Indeed, active and reactive power outputs from DGs relying only on the droop control could differ from those equipped with secondary and/or tertiary controls, because the two higher levels will adjust operating points of a microgrid. Specifically, the tertiary control level is similar to economic dispatch control in the context of bulk power systems and typically executes every few minutes. On the other hand, the secondary control provides a correction to the primary control and these two levels can run on a closer time scale (i.e., every few seconds). As noted earlier, the tertiary management level incorporates load forecasting and then establishes dispatch curves for each DG on an economic basis. Since this stage runs on a longer time scale, it is considered to provide a nearly constant reference seen from the secondary and primary levels. The secondary level of each DG attempts to track the economic dispatch commands as closely as possible, which is facilitated by PI controllers with negligible computation as in (3).

## III. STRUCTURE OF POTSDAM MICROGRID

This section describes the Potsdam Resilient Underground Microgrid, which will provide power supply to selective entities within the village of Potsdam continuity when natural disasters strike. As shown in Fig. 1, this microgrid consists of a 13.2-kV underground distribution network connecting included entities together on a dedicated ring. The underground grid is more resilient against weather-related events than overhead lines, although it is more expensive to install and maintain. When in grid-connected mode, a combination of DGs within the microgrid is able to supply power to the local loads and excess power, if any, will be injected to the main grid. The existing overhead feeder serving Clarkson University Campus is identified as the primary connection by National Grid. Should this feeder not be available, there are five other secondary overhead connections that would allow this microgrid to operate in grid-connected mode. When the underground microgrid is disconnected from the overhead grid, the connected entities can be powered by on-site DGs. Nevertheless, a load shedding plan should be implemented in order to balance generation/load and to allow for a secure generation margin.

Two types of DERs were considered when designing the Potsdam Microgrid, in which conventional DERs (e.g., natural gas generators and micro-turbines) are connected to the 13.2-kV ring-configured distribution network, while renewable DERs (e.g., solar panel) are interfaced through

voltage source converters (VSC). In this distribution network, only the DGs and load at Bus 9 are directly connected to the 13.2-kV line, while all others are connected through step-up transformers rated 4.8/13.2 kV. To regulate voltage, two static var compensators are deployed at Buses 7 and 9 respectively. The detailed system data is available in [13].

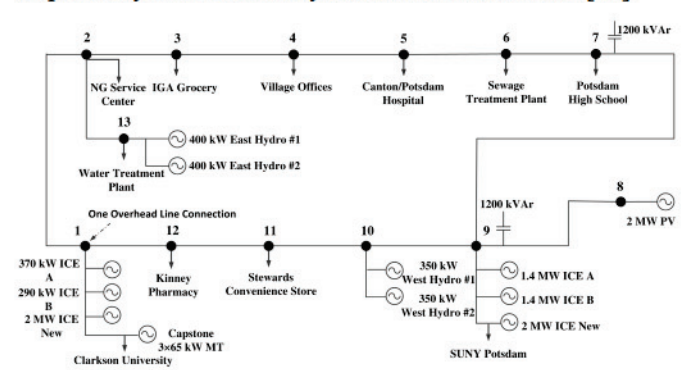


Figure 1. One-line diagram of the Potsdam Microgrid

### IV. SIMULATION RESULTS

In this section, two cases are simulated in PSCAD/EMTDC to study the optimal control of the Potsdam Microgrid. One is to study the islanding process, forming the technical basis for our main research. Indeed, the islanding capability of a microgrid is expected to come into play during disasters when the main grid fails. The other case is concerned with the optimal control of the community microgrid after the successful islanding. The total rated demand is 9.846 MW at 0.85 power factor.

In terms of the control schemes, the PV array at Bus 8 is equipped with energy storage devices and therefore can be operated in the constant PQ mode, and the Capstone microturbines at Bus 1 are also PQ controlled; other DGs are represented by inverter-based models and are operated in the droop mode. Besides static load models that are both frequency and voltage dependent [14], two dynamic loads at Buses 6 and 13 are modeled as wound rotor induction motors. Load forecasting is beyond the scope of this research. Nevertheless, forecasting methods such as regression models can be developed based on historical or simulated load data. In this paper, load profiles are assumed to be projected by a data center beforehand and will be used as inputs for the EMS module in PSCAD/EMTDC.

## Case 1: Unintentional Islanding

Initially the microgrid is importing 0.92 MW from and exporting 2.54 Mvar to the main grid. All the DGs but the PV array are operated close to their nominal ratings. At t = 1 sec, the circuit breaker on the primary overhead feeder is automatically opened due to a fault on the main grid, and the islanding takes place. Fig. 2 shows active power generations of several representative DGs before and after islanding. Since the frequency begins to drop, all the DGs on the droop control will increase their power outputs. For example, the 370-kW ICE Fuel Generator A at Bus 1 supplies more than

its nominal power level and experiences a 1.5-times overloading during a transient state. With appropriate load shedding, the DGs would be sufficient to meet active power demand with certain margin. At t = 1.2 sec, load shedding is initiated. For the sake of discussion, we consider curtailed loads are only taken from Clarkson University and SUNY Potsdam, i.e., 1 MW out of the original 4.7-MW load at Clarkson, and 0.8 MW out of the original 4.1-MW load at SUNY Potsdam. Afterwards, the system frequency rises. Correspondingly, each DG on the droop control will decrease its power output. It can also be seen in Fig. 2 that each DG in the droop control mode picks up the load change roughly proportional to their active power ratings subsequent to another transient state. Meanwhile, active power output of the PV keeps nearly constant because it is PQ-controlled.

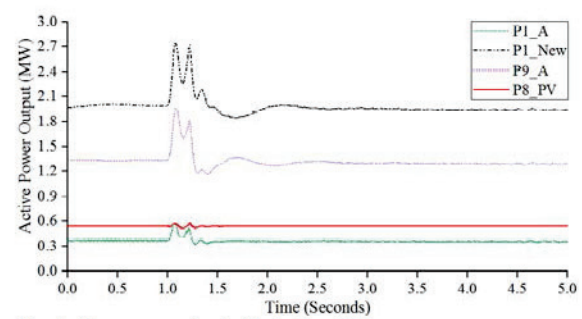


Figure 2. Active power output of selective DGs

Case 2: Optimal Control and Operation During Islanding

Case 1 demonstrates effectiveness of the hierarchical control scheme that utilizes droop control to ensure proper active load sharing during the transition to the islanding mode. In this case, we proceed to study the optimal control of this microgrid in islanded mode by incorporating secondary and tertiary levels. A PSCAD/MATLAB interface is developed, which functions as the EMS module. The SDP based ACOPF is conducted in MATLAB invoking the MOSEK optimizer. Numerical experiments show that the SDP based ACOPF obtains an optimal solution in most cases and the computation takes less than 1 second. In this study, the ACOPF problem is solved in every two seconds and the optimal active power dispatch is then determined.

We propose two methods to track the optimal dispatch commands, both of which start at t=3 sec in the simulation. Method 1 makes PI control continually act, whereas Method 2 resets PI output to zero periodically, e.g., every two seconds in this case, to prevent system frequency from constantly increasing or decreasing. Figs. 3-4 display the optimal dispatch command and the actual power output response of selective DGs in the two methods. System frequency and the total cost curves are presented in Figs. 5 and 6.

Throughout the numerical optimization we obtain that the two ICE fuel generators at Bus 1, namely A and B, and the two hydro generators at Bus 10 should be fully loaded due to their relatively lower operating costs. Fig. 3 illustrates how ICE fuel generator A at Bus 1 tracks the economic dispatch

command issued by the EMS module. The largest deviation (i.e., 4.9%) in Method 1 arises around t = 7.3 sec. In comparison, this DG experiences small power oscillation due to reset action in Method 2. Fig. 4 shows that hydro generator A at Bus 9 keeps tracking its economic targets as closely as possible when using either method, while Method 1 allows smoother control. Overall, the first method shows better tracking performance since it smoothly tracks dispatch commands. On the other hand, power output using Method 2 experiences periodical transients, although system frequency is under control, as shown in Fig. 5. It should also be noted that the Capstone micro-turbines and the PV array can perfectly track their optimal economic dispatch curves since they are both PQ-controlled. Fig. 6 further shows that Method 1 generates lower actual cost in most time.

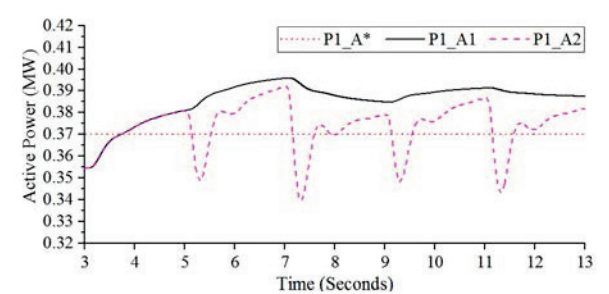


Figure 3. Performance of ICE generator A at Bus 1 via the two methods

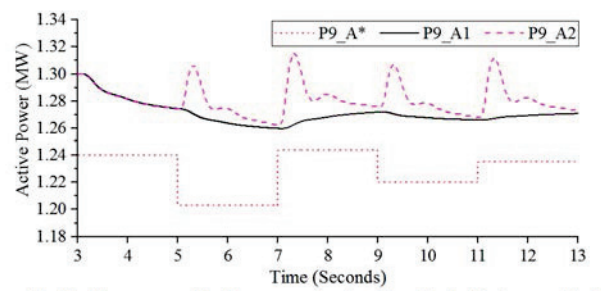


Figure 4. Performance of hydro generator A at Bus 9 via the two methods

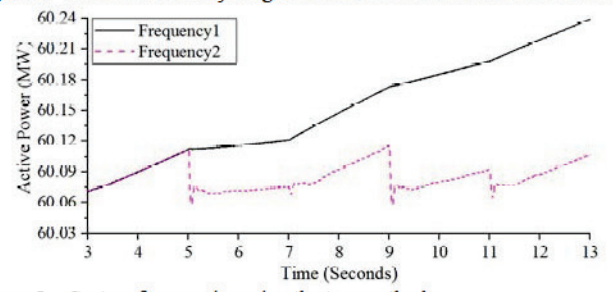


Figure 5. System frequencies using the two methods

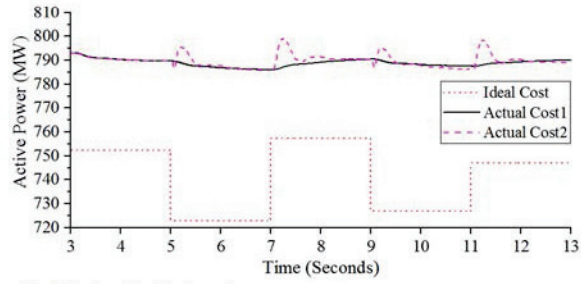


Figure 6. Ideal and actual cost curves

## V. CONCLUSIONS

This paper adopts the three-level hierarchical control scheme to evaluate the performance of the designed Potsdam Underground Microgrid in islanded mode. Coordination among the three levels is also discussed. Numerical simulations show that after the ACOPF problem is solved on the tertiary level, the two proposed secondary control methods enable DGs on droop control to closely track economic targets. While system frequency is not a controllable variable in the first method, a better tracking performance can be obtained when compared with the second method, due to smooth PI control. Future work would explore robust three-level hierarchical control strategies to mitigate load forecasting inaccuracies and other uncertainties. In addition, dynamic demand response and multi-party business models will also be considered.

#### REFERENCES

- Lei Wu, Tom Ortmeyer, and Jie Li, "The Community Microgrid Distribution System of the Future," *The Electricity Journal*, 29 (10), pp. 16-21, December 2016.
- [2] Lei Wu, Jie Li, Melike Erol Kantarci, and Burak Kantarci, "An Integrated Reconfigurable Control and Self-Organizing Communication Framework for Community Resilience Microgrids," *The Electricity Journal*, 30 (4), pp. 27-34, May 2017.
- [3] Jie Li, Yikui Liu, and Lei Wu, "Optimal Operation for Community-Based Multi-Party Microgrid in Grid-Connected and Islanded Modes," *IEEE Trans. Smart Grid*, vol. 9, no. 2, pp. 756-765, March 2018.
- [4] Yang Han, Hong Li, Pan Shen, Ernane Antonio Alves Coelho, and Josep M. Guerrero, "Review of Active and Reactive Power Sharing Strategies in Hierarchical Controlled Microgrids," *IEEE Trans. Power Electronics*, vol. 32, no. 3, pp. 2427-2451, March 2017.
- [5] Daniel E. Olivares, Ali Mehrizi-Sani, Amir H. Etemadi et al., "Trends in Microgrid Control," *IEEE Trans. Smart Grid*, vol. 5, no. 4, pp. 1905–1919, July 2014.
- [6] J. A. Momoh, Electric Power System Applications of Optimization. New York: Markel Dekker, 2001.
- [7] Xiaoqing Bai, Hua Wei, Katsuki Fujisawa, and Yong Wang, "Semidefinite programming for optimal power flow problems," International Journal of Electrical Power & Energy Systems, vol. 30, Issues 6–7, pp. 383-392, July–September 2008.
- [8] Javad Lavaei, and Steven H. Low, "Zero Duality Gap in Optimal Power Flow Problem," *IEEE Trans. Power Systems*, vol. 27, no. 1, pp. 92-107, February 2012.
- [9] Javad Lavaei, David Tse, and Baosen Zhang, "Geometry of power flows in tree networks," in *Proc.2012 IEEE PES General Meeting*, pp. 1-8
- [10] N. Pogaku, M. Prodanovic, and T. C. Green, "Modeling, analysis and testing of autonomous operation of an inverter-based microgrid," *IEEE Trans. Power Electronics*, vol. 22, no. 2, pp. 613–625, March 2007.
- [11] J. W. Simpson-Porco, Q. Shafiee, F. Dörfler, et al., "Secondary Frequency and Voltage Control of Islanded Microgrids via Distributed Averaging," *IEEE Trans. Ind. Electron.*, vol. 62, no. 11, pp. 7025– 7038, Nov. 2015.
- [12] A. K. Basu, A. Bhattacharya, S. Chowdhury, and S. P. Chowdhury, "Planned scheduling for economic power sharing in a CHP-based micro-grid," *IEEE Trans. Power Systems*, vol. 27, no. 1, pp. 30–38, Feb. 2012.
- [13] H. Wiegman, "Microgrid Plant Control Design and Development," GE Global Research, Niskayuna, NY, Tech. Rep. DE-OE0000728, July 2017.
- [14] P. Kundur, Power System Stability and Control, New York: McGraw-Hill, 1994, p. 272.